Biophysical principles predict fitness of SARS-CoV-2 variants

DIANZHUO WANG[1,2], MARIAN HUOT[1,3], VAIBHAV MOHANTY [1,4] AND EUGENE I. SHAKHNOVICH[1,*]

[1] *Department of Chemistry and Chemical Biology, Harvard University, Cambridge, MA*
[2] *John A. Paulson School of Engineering and Applied Sciences, Harvard University, Cambridge, MA*
[3] *Ecole Polytechnique, Institut Polytechnique de Paris*
[4] *Harvard-MIT MD-PhD Program and Program in Health Sciences and Technology, Harvard Medical School, Boston, MA and Massachusetts Institute of Technology, Cambridge, MA*
[*] *shakhnovich@chemistry.harvard.edu*

Abstract: SARS-CoV-2 is under constant selective pressure from antibodies while requiring efficient binding to host cells for successful infection. Here we focus specifically on the receptor binding domain (RBD) of the SARS-CoV-2 spike protein, a key determinant of viral entry into host cells. Through a comprehensive approach, comprising large-scale sequence analysis of SARS-CoV-2 variants and the formulation of a fitness function based on protein folding and binding thermodynamics, we unravel the relationship between the epidemiological fitness contribution of the RBD and its biophysical properties. We developed a biophysical model mapping the phenotype space, characterized by binding constants to cell receptors and antibodies, onto the fitness landscape for variants ranging from the ancestral Wuhan Hu-1 to the Omicron BA.1 . Using equilibrium statistical mechanics, we show how fitness can be expressed as a function of binding constants to cell receptors and antibodies and validate our findings through experimentally measured binding affinities and population data on frequencies of variants. This forms the basis for a comprehensive epistatic map, relating the genotype space to fitness. Our study thus delivers a tool for predicting the fitness of variants harboring previously unseen mutations, and sheds light on the impact of specific mutations on viral fitness. These insights offer not only greater understanding of viral evolution but also potentially aid in guiding public health decisions in the battle against COVID-19 and future pandemics.

1. Introduction

Since its emergence, the SARS-CoV-2 virus has undergone continuous genetic changes, giving rise to variants with increased transmissibility such as Alpha, Delta, and the recent Omicron. Each has contributed to significant surges in global COVID-19 cases. These genetic alterations in the viral genome have a profound impact on the structure and function of viral proteins, causing consequential changes in viral fitness (defined as the capacity of the virus to reproduce). Variants of concern, such as Omicron, possess specific mutations in the spike protein. They have been linked to enhanced transmissibility [1, 2], augmented binding to host cell receptors, and heightened resistance to antibody neutralization. [3, 4]. Understanding the relationship between these mutations and viral fitness requires investigating their influence on molecular properties of affected proteins. Key viral proteins, like the receptor binding domain (RBD) of the spike protein, play a critical role in facilitating viral entry into host cells by binding to angiotensin-converting enzyme 2 (ACE2) [5], a functional receptor on cell surfaces. What's more, RBD serves as primary targets for the most potent SARS-CoV-2-neutralizing antibodies [6]. Therefore, mutations on the RBD have been shown to be highly correlated with increases of fitness.

On the experimental side, Starr et al. [7] systematically scanned through every amino acid substitution in the RBD of the spike protein to determine the mutation effect on RBD folding and ACE2 binding and showed a substantial number of mutations are well tolerated or could even enhance ACE2 binding. In more recent research, Moulana et al. [8, 9] conducted a thorough examination of the binding affinity across all combinations of the 15 RBD mutations found in the BA.1 variant of SARS-CoV-2 in comparison to the original Wuhan Hu-1 strain. This exploration covered a total of 32,768 genotypes and involved testing against four monoclonal antibodies (LY-CoV016, LY-CoV555, REGN10987, and S309) as well as the ACE2 receptor. Additionally, global initiatives that promote data sharing, such as the Global Initiative on Sharing All Influenza Data (GISAID) [10], provide us with the ability to derive viral fitness based on prevalence data.

Prior research has derived a quantitative correlation between fitness and molecular properties. For instance, Cheron et al. [11] and Rotem et al. [12] devised a theoretical framework to assess fitness of RNA viruses and validated it using experimental and computational methods. Central to their premise is that fitness comes from the proportion of viral capsid proteins in folded state free of antibodies, with state-occupation probability determined from Boltzmann distribution. SpikePro, a computational model, uses the spike protein's amino acid sequence and structure to estimate SARS-CoV-2 fitness. The model takes into account the stability of the spike protein, its binding efficiency with ACE2, and the potential for immune evasion [13]. While it has shown effectiveness in identifying dominant viral strains, it is worth noting that this is an empirical model whose foundation is not grounded in biophysical principles. Furthermore, there is an absence of experimental verification for the model's predictions, which highlights the need for more rigorous, physics-based models.

The central aim of our study is thus to bridge the gap between viral fitness and biophysical properties of the RBD. We concentrate specifically on how emerging mutations affect both the fitness and the binding energies of the RBD to ACE2 and antibodies, as illustrated in Fig.1. By doing so, we aim to develop a robust methodology based on statistical mechanics to forecast RBD fitness anchored in its binding affinities with ACE2 and antibodies.

This study establishes a biophysical link between binding affinities and relative fitness for SARS-CoV-2 mutants. To that end, we have constructed a genotype-to-fitness mapping for the SARS-CoV-2 RBD under the constraints of successful cellular entry via ACE2 and influence of neutralizing antibodies. This mapping equips us with a predictive tool for assessing the fitness of emerging SARS-CoV-2 variants.

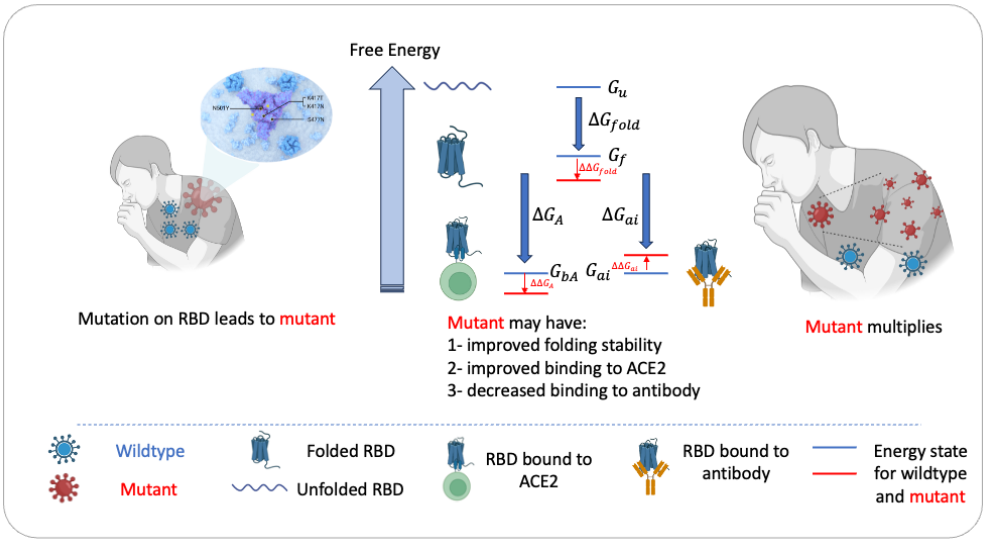

Fig. 1. High fitness variants may exhibit improved stability in the folded state or in the ACE2-bound state to facilitate cellular entry or have the capacity to destabilize bound-to-antibody states, thereby enabling evasion.

2. Results

2.1. The model

Our RBD fitness function is based on thermodynamics of protein folding and binding. We consider fitness, denoted F, as proportional to the fraction of RBD that are folded and free from antibodies. Specifically, we assume a seven-state microscopic configuration model for the RBD: unfolded, folded and unbound, folded and bound to ACE2, and folded and bound to one of four different antibodies, with respective free energies G_u, G_f, G_{bA} and G_{ai}, where i is an index over the 4 antibodies. In our model, the RBD can only be bound to one antibody at a time, or ACE2 and to no antibody, or be free from ACE2 and antibodies. We then assume that an RBD can exist at thermodynamic equilibrium over these 7 states at some finite temperature T_s, denoted by $\beta = 1/(k_B T_s)$, where k_B is the Boltzmann constant. Following [12], we then propose that fitness F, which in our context signifies the contribution to the viral growth rate from the RBD, is proportional to the Boltzmann probability of RBD being found in the folded state free from antibodies or in the folded, bound to ACE2 state. Thus, fitness F can be expressed as

$$F \propto \frac{Ce^{-\beta G_{bA}} + e^{-\beta G_f}}{Ce^{-\beta G_{bA}} + \Sigma_i C_i e^{-\beta G_{ai}} + e^{-\beta G_f} + e^{-\beta G_u}} \tag{1}$$

In this equation, $C = \frac{[ACE2]}{C_0}$ and $C_i = \frac{[Ab_i]}{m_i C_0}$ where $[\ldots]$ represents concentration. m_i accounts for the quantity of antibodies required to neutralize the virus. The use of the standard reference concentration C_0 allows us to express C and C_i in dimensionless form. For each mutant mut, the relative fitness compared to the wildtype wt (Wuhan-Hu-1), defined as $\frac{F_{mut}}{F_{wt}}$, follows the same relationship as the absolute fitness and will be studied in the following work. To avoid confusion, we will simply refer to this relative measure as the "fitness" F. Defining free energy differences between states as $\Delta G_{fold} = G_f - G_u$, $\Delta G_A = G_{bA} - G_f$ and $\Delta G_{ai} = G_{ai} - G_f$, we get:

$$F = a\frac{Ce^{-\beta\Delta G_A} + 1}{Ce^{-\beta\Delta G_A} + \Sigma_i C_i e^{-\beta\Delta G_{ai}} + e^{\beta\Delta G_{fold}} + 1} \tag{2}$$

where a is a scaling factor. Finally, given that RBD domains are stable - with the unfolded states having significantly higher free energy than the folded states (that is, $e^{\beta\Delta G_{fold}} << 1$, see "Methods") - we can simplify the model as follows:

$$F = a\frac{Ce^{-\beta\Delta G_A} + 1}{Ce^{-\beta\Delta G_A} + \Sigma_i C_i e^{-\beta\Delta G_{ai}} + 1} \tag{3}$$

Noting that, $\Delta G \propto ln(K_D)$, we get fitness can be expressed as a logistic function of the log of dissociation constants K_{DA} and K_{Dai} for ACE2 and antibodies (see "Methods" for Eq. 4). Our study is centered on inferring F by fitting a scaling parameter a and effective population concentrations C and C_i to the biophysical model. In our model, the temperature is treated as a hyperparameter that can be tuned (see "Methods" and SI for details). For clarity, a summary of all the symbols is provided in Table 1.

2.2. Fit of biophysical model to fitness obtained from population data

We categorized our data based on the presence or absence of the T478K mutation (see "Methods" for explanation of the rationale behind such categorization) and separated it into training and testing sets (see "Methods"). We calibrated our biophysical model using observed viral variants [14] (see "Methods" for the details on conversion of population data into fitness) from the population study and incorporated experimental measurements of binding affinities [8, 9] as an input. Training of the model involved adjusting **6** parameters (a, C, and C_i for i ranging from 1 to 4) to achieve highest correlation between model prediction Eq. (4) and fitness inferred from population data in the training set.

Initially, we trained our model on 80% of the observed variants, achieving a highly satisfactory fit (R^2 = 0.94). This result was further corroborated by the high accuracy predictive power demonstrated on the test set (R^2 = 0.95), thus confirming the absence of over-fitting (Figure 2b). Our model's performance reflects the biophysical understanding that a combination of strong ACE2 binding and reduced antibody binding could provide the virus with a fitness strategic advantage, enhancing its ability to penetrate cells.

To further explore the behavior of our model, we fixed all but one of the dissociation constants at their mean value across mutants, and studied the variation of inferred relative fitness as a function of the unfixed constant. Interestingly, we observed that variants carrying a combination of Omicron mutations consistently fell into the upper plateau or linear segment of our biophysical model (Figure 2c). This suggests that natural selection did not favor combinations of mutations that would lead to high antibody binding. It should be noted that in each curve on Figure 2c, four out of five dissociation constants are fixed. Thus, the inferred fitness for each data point in these one-dimensional cross sections of the fitness landscape does not represent its actual fitness.

Further validation of the robustness of our model was undertaken by applying it to ten non-overlapping subsets of observed variants (Figure 2d). The error bars illustrate minor variations in coefficients, indicating the model's stability. Moreover, the coefficients for datasets, both with and without the T478K mutation, were remarkably similar. Intriguingly, the effective concentrations derived from our model for antibody binding demonstrated remarkable consistency across LY-CoV016, LY-CoV555, and REGN10987. A notable exception was the coefficient corresponding to the S309 antibody, which continues to be effective across a range of variants, from the original Wuhan strain to Omicron BA.1, thereby preventing viral immune escape. This unique attribute of S309 is represented in our model as a relatively higher effective concentration.

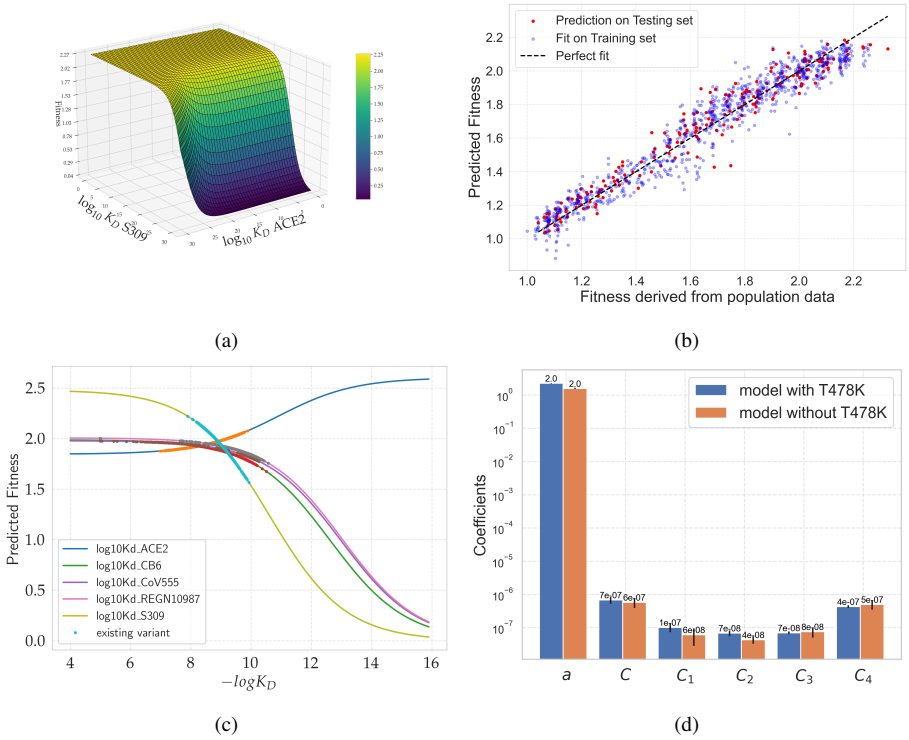

Fig. 2. Biophysical Model Analysis. (a) A slice of the fitness landscape that reveals the relationship between inferred fitness and the logarithm of the ACE2 and antibody S309 dissociation constants. (b) Model performance with fitness predictions versus true fitness values. (c) The dependence of the fitness function on the logarithm of each dissociation constant. Data points representing existing variants are presented as dots. (d) A bar plot of the fitted coefficients from the biophysical model, presenting variants with and without the T478K mutation.

2.3. Predictive power of the biophysical model

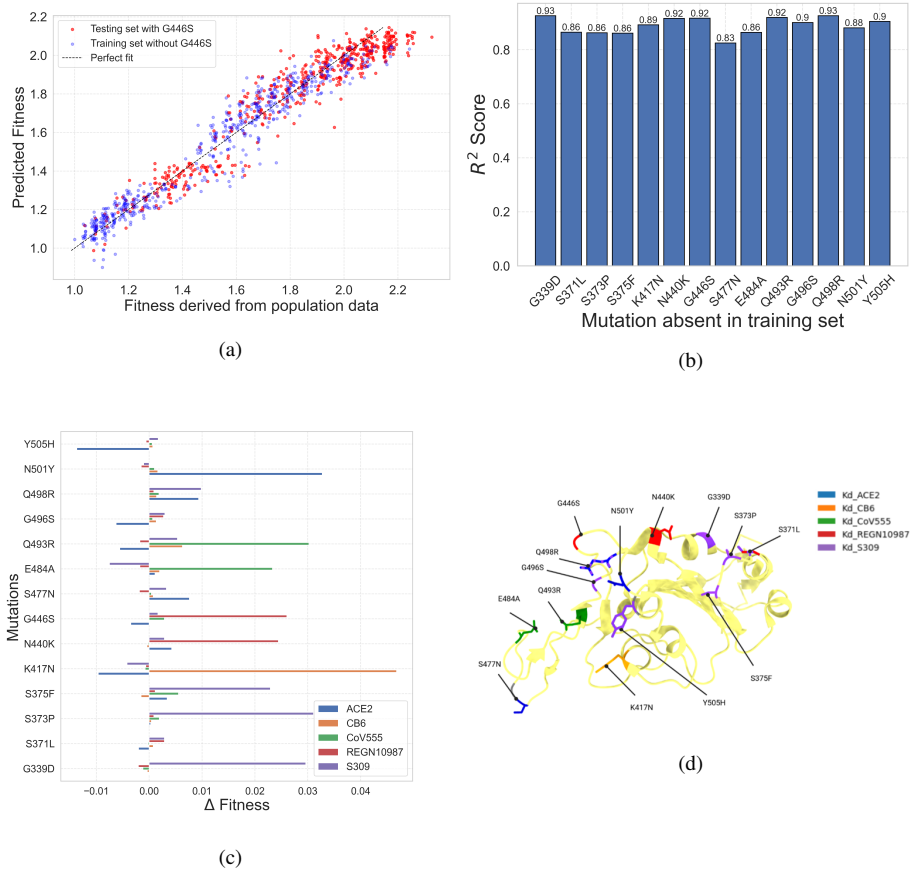

Fig. 3. Assessing Predictive Power of the Model. (a) Fitness prediction for variants carrying the G446S mutation which was not included in the training set yields $R^2 = 0.92$ (b) R^2 derived from a model trained on variants excluding a specific mutation, then used to predict the fitness of variants exhibiting that mutation. (c) Contributions of each mutation to fitness either towards evading specific antibodies or facilitating cellular entry. (d) A crystal structure of the wild-type RBD, with Omicron substitutions indicated. Mutated residues are color-coded based on the largest fitness contribution associated with the mutation. Bi-color representations suggest that two features contribute equally to fitness.

Our model constitutes an effective tool for forecasting the fitness of entirely novel viral lineages, given molecular properties of their RBD domain. The model's potential manifested in its ability to predict fitness of unobserved variants accurately. This evidence underscores the model's power in predicting the impact of novel mutation combinations, as shown in Figure 3a.

This point is further highlighted in Figure 3b. For each mutation, labeled as m, our model was systematically trained on all variants that exclude mutation m and then used to predict fitness of all existing variants carrying mutation m in combination with other possible mutations. This methodology, implemented across all 14 mutations, yielded a strong R^2 coefficient of over 0.8. Remarkably, our model even succeeds in predicting fitness of variants bearing the novel G446S mutation, a demanding task considering that this mutation chiefly causes escape from the

REGN10987 antibody [9].The model's ability of predicting the impact of the G446S mutation on fitness, despite the complexity of correlating complete immune escape from REGN10987 to fitness, highlights the practical potential of our model in real-world scenarios. Significantly, while our model has been trained on mutations spanning from the Wuhan variant to the Omicron variant, it's not restricted to this specific spectrum. The model exhibits the capability to capture the effects of mutations outside the scope of Wuhan to Omicron, provided the relevant RBD's biophysical properties are available, either through experimental data or simulations.

Finally, through the Taylor expansion of our biophysical model (see "Methods" and SI), we can translate the observed improvements in ACE2 binding or immune escape (i.e., changes in binding constants) of specific variants compared to the wild type into alterations in fitness for each individual mutation. In Figure 3c, we have quantified the individual contributions of each mutation towards either the evasion of specific antibodies or the binding to ACE2, thus unravelling the complex landscape of viral adaptation strategies.

In Figure 3c, we observe that the fitness effects for each mutation is primarily associated with one or two biophysical parameters. Furthermore, mutations spatially close on the spike protein often share similar characteristics contributing to their fitness. This observation is graphically represented on the crystal structure in Figure 3d.

2.4. Epistasis

Previous work of Moulana et al. [9] showed that mutations involved in antibody escape generally lead to a decrease in the affinity of the virus for ACE2 receptors, suggesting that the evolution of the virus was limited by a trade-off between evading the immune response and maintaining its ability to enter host cells. This trade-off gives rise to a phenomenon called epistasis, where the effect of one mutation depends on the presence of other mutations. Specifically, we observed that there exists a threshold for total fitness of the RBD, beyond which additional mutations do not further increase fitness. [15] In other words, once the virus reaches a certain level of fitness due to high immune escape and relatively tight binding to cell receptor, it becomes more difficult for additional mutations to keep improving this balance and fitness starts to plateau (Figure 4a), a phenomenon which was not inferred by Obermeyer et al. [14] or other non-epistatic models.

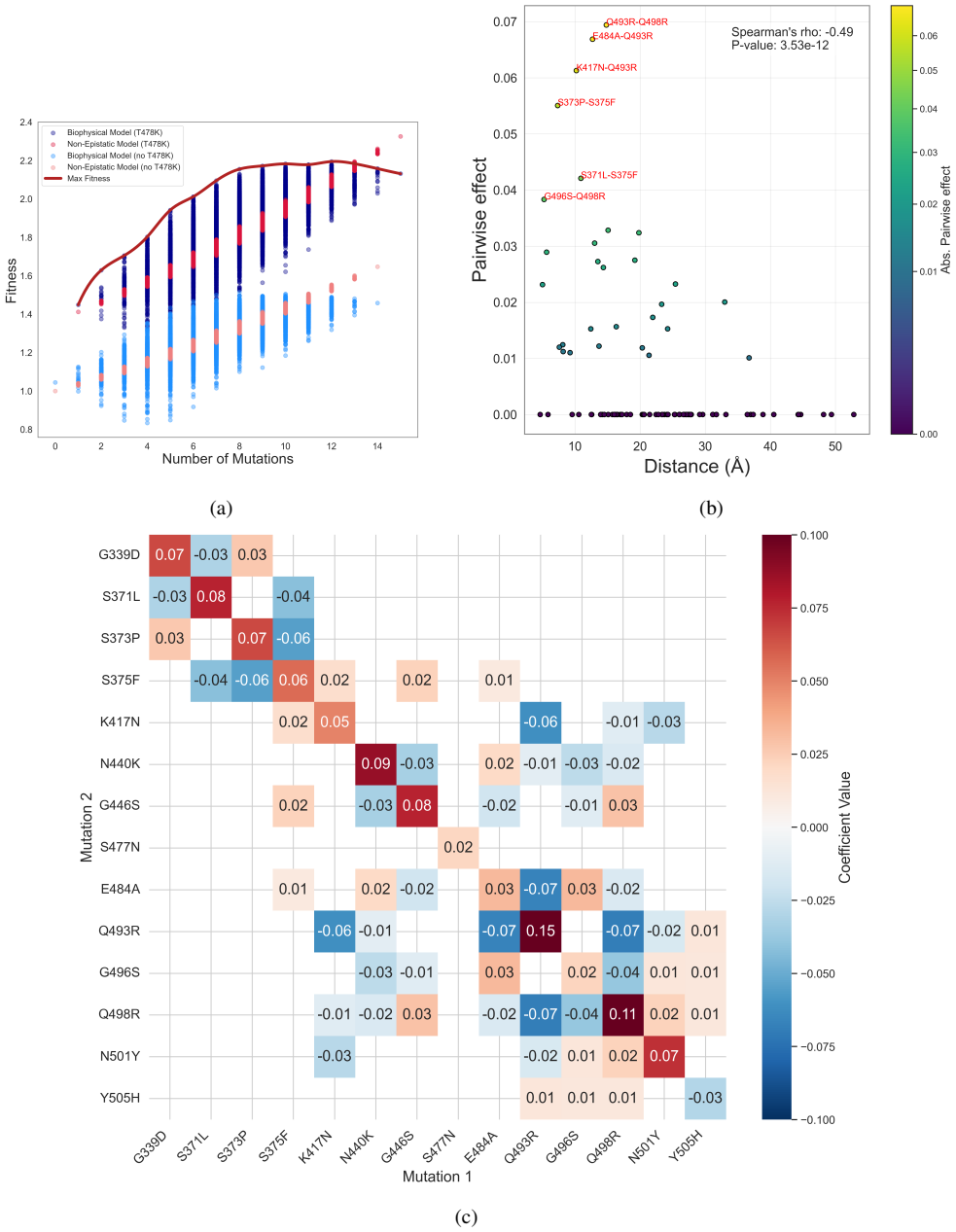

Fig. 4. Epistasis Analysis. (a) Predicted fitness values with the non-epistatic model of Obermeyer et al. and with our epistatic biophysical model, highlighting the plateau effect. (b) Pairwise (second order) interaction coefficients against the spatial distances between the corresponding residues, with mutations colored in accordance with the absolute value of their pairwise coefficient. (c) Coefficients of epistasis: diagonal coefficients denote first order interactions, whereas off-diagonal coefficients represent second order interactions. Coefficients smaller than 0.01 have been masked for clarity.

To calculate the epistatic coefficients, we utilized a linear model in which the effects of mutation combinations summed to the phenotype of a sequence (see "Methods: Epistasis analysis" for

definitions and details). We then applied this model to fitness values inferred from our biophysical model across all 32,768 possible combinations of mutations. The performance of the model was evaluated (expressed as the coefficient of determination, R^2) for different orders of epistasis on a withheld test dataset, constituting 10% of the total data. A first-order model (comprising 16 coefficients) produced an R^2 value of 0.96, while a second-order model (comprising 121 coefficients) achieved an R^2 of 0.98. The high correlation values and satisfactory representation of the data suggest that a second-order model sufficiently captures the key dynamics, thereby alleviating the necessity for higher-order models.

These high correlation values are attributable to our model's ability to fit to real fitness coefficients obtained in a non-epistatic model from Obermeyer et al. [14]. Despite this, our biophysical model successfully captures epistatic effects as it is based on the dissociation constants of the RBD to antibodies and ACE2, which inherently exhibits epistatic behavior. Following the training of the second-order model across the complete dataset to derive final coefficients, we observed that most single mutations (reflected on the diagonal of the matrix in Figure 4c) have a positive impact on fitness. Interestingly, one mutation, Y505H, exhibited a negative first-order coefficient, which is nonetheless offset by epistasis.

We discovered that mutations with a pronounced effect on antibody escape—specifically K417N, G446S, E484A, and Q493R [8]—individually confer high fitness. However, the co-occurrence of all four mutations results in a marked fitness detriment due to the consequent reduction in affinity to ACE2. This finding highlights the balancing act between immune escape and receptor binding in viral evolution. Lastly, we observed that certain adjacent mutations, particularly S373P/S375F and E484A/Q493R/Q498R, interact in a non-additive manner, leading to deleterious effects (Figure 4b).

These findings underscore the complex dynamics of viral evolution, in which multiple concurrent mutations can bolster viral fitness via various pathways. This intricate balance of positive and negative selection pressures enhances the likelihood of co-selection of mutations. Consequently, our results highlight the necessity of considering the interactive effects of multiple mutations, rather than considering mutations in isolation, when modeling and predicting viral evolution.

3. Discussion

Although the complexity of fitness landscapes is undeniable, recent research indicates that in certain biologically and clinically significant systems, such as evolution of bacterial resistance against antibiotic [16], evolution of viral resistance against antiviral treatments [11, 17], as well as norovirus evolution against a neutralizing antibody [12], these fitness landscapes can be systematically and quantitatively delineated. Our research builds upon these findings and reveals that the fitness landscape of the SARS-CoV-2 RBD, undergoing evolution against neutralizing antibodies, can be systematically elucidated through its biophysical properties. In our study, we found the strength of binding to the neutralizing antibody, as well as to ACE2, play crucial roles in determining RBD fitness. The relevance of these biophysical parameters extends to other viruses as well. For instance, both binding affinity for antibodies [18] and protein folding stability [17, 19] have been identified as important traits influencing the evolution of influenza viruses.

By correlating the fitness landscape with explicit biophysical properties, we have quantified the influence of evolutionary forces acting upon it. In the context of antibodies targeting the receptor binding site, the virus must perform a delicate balancing act: necessary mutations must instigate sufficient antigenic change without compromising receptor binding function. Consequently, we observe a tendency for fitness to plateau in the face of increasing number of mutations relative to the wild type, which we attribute to the negative epistasis introduced as mutation count rises. This phenomenon of diminishing returns, manifested as a fitness plateau, has been extensively

studied in existing literature [15, 20–23]. It aligns with the theoretical work of Lyons et al. [24] which suggested that when epistasis is partially idiosyncratic (due to pairwise effects), a negative correlation is anticipated between fitness of the existing genetic background and the mutational effect, encapsulating the concept of diminishing returns from beneficial mutations.

Despite our biophysical model being trained on non-epistatic population data from Obermeyer et al. [14], predicting viral fitness using the experimental data allows us to generate an epistatic map from genotype to fitness. Our results indicate that epistasis significantly constrains evolution, with certain mutations tolerated only after the occurrence of others. While many of the mutations we investigated are beneficial, specific combinations of mutations could be deleterious. These mutations require the prior or concurrent occurrence of stabilizing mutations to counterbalance their adverse consequences. This observation is consistent with findings of Gong et al. [17] and Rodrigues et al. [25] underscoring the critical role of stabilizing mutations in fixation of subsequent destabilizing mutations that could hold adaptive value.

Our research presents a physical model centered around fitness derived from mutations on the RBD. By exclusively utilizing experimentally derived biophysical parameters, our model can accurately predict the fitness of new RBD variants, thereby providing valuable insights into their potential proliferation within populations. Considering the RBD's known susceptibility to mutations, our model could be instrumental in forecasting the growth trajectory of new variants before they emerge as significant threats, granting public health officials invaluable time for planning and adaptation. The potential applications of our work also include the use of simulation-based approaches such as molecular dynamics to predict with high accuracy these binding constants for new emerging variants leading potentially to possibility of proactive interventions.

A fundamental premise of our model is that the fitness of the SARS-CoV-2 virus is predominantly determined by its capacity to bind to the ACE2 receptor and evade antibodies. The model based on this premise demonstrates the ability to predict the fitness effect of all mutations, barring T478K. This is in line with previous studies by Moulana et al. [8, 9] which indicated that the T478K mutation had a negligible effect on dissociation constants, despite its strong contribution to variant growth rate. This justifies our decision to segregate the data based on the presence of this mutation, and to account for its impact by increasing the scaling coefficient in our biophysical model.

Based on these results, extrapolating our fitness predictions using biophysical data to encompass the full COVID sequence, or even the entire Spike protein, presents a challenge. It is likely that mutations outside the RBD will have effects that extend beyond alterations to binding constants with cell receptors and antibodies, complicating the predictions.

Furthermore, our model currently considers antibody binding to just four monoclonal antibodies, an oversimplification given the complexity of human immune responses. While our model already exhibits highly accurate predictions, the inclusion of additional factors such as other antibodies, vaccination effects, the replicative capacity within the infected cell [26], transmission dynamics [27], and drug resistance [28] could potentially enhance its predictive power and realism.

4. Methods

4.1. RBD Fitness Data analysis

We acquired the fitness ratio of each RBD compared to wild type from the work of Obermeyer et al. [14]. In their study, the fitness label is obtained by modeling the relative growth rate of SARS-CoV-2 lineages using a hierarchical Bayesian regression model. The model combines individual mutations and clusters genetically similar genomes to estimate the incremental effect of amino acid changes on growth rate within each lineage, which enables the model to share statistical strength among similar lineages. Specifically, the proportion of lineages is modeled

as a multinomial distribution whose probability parameter is a multivariate logistic growth function softmax $(\alpha + tb/\tau)$. For each lineage, the slopes b are linearly regressed against the presence of each possible amino acid substitution $X_m \in \{O, 1\}$ as $b = \sum_m b_m X_m$. These linear coefficients b_m can be directly interpreted as the effect of a mutation m on a lineage's fitness. This model assumes each single point mutation independently linearly contributes to change in fitness. Authors reported that fitting a similar model of both single and pair mutations lead to no pairwise mutations stronger than the top 100 single mutations.

This enabled us to estimate the fitness F_{mut} of each existing RBD mutant, compared to wildtype. Using $b = \log(\frac{F_{mut}}{F_{wild}})$, we get:

$$\frac{F_{\text{mut}}}{F_{\text{wild}}} = \exp\left(\sum_{m \in \text{RBD}} b_m X_m\right)$$

4.2. RBD Binding Affinity

We acquired the binding affinity data from the work of Moulana et al. [8, 9] In their study, they systematically examined the interactions between all possible combinations of 15 RBD mutations (totaling 32,768 genotypes) and ACE2, as well as four monoclonal antibodies (LY-CoV016, LY-CoV555, REGN10987, and S309) via Tite-seq measurement. In situations where binding affinities in their dataset were too low to measure accurately, we have chosen to substitute these with a fixed value of 5. We stress that this choice of value is not expected to influence our study's outcomes. As indicated in Figure 2c, the antibody escape largely resides in the upper plateau region of the fitness curve, thus, this preset value for variants with immune escape to antibodies does not have a substantial impact on the logistic regression results. Furthermore, we eliminated approximately 100 genotypes from the analysis that did not have measured ACE2 binding affinity.

4.3. Effect of mutations on RBD stability

In the presented results, we excluded the unfolded state from the model, on the assumption that this variable shows minimal variation across different variants and hence, would not significantly influence fitness. To verify this assumption, we employed DDGUN, an untrained, high-throughput tool [29], to compute $\Delta\Delta G_{fold}$, the variance in folding free energy difference, for mutants relative to the wild-type: the maximum variation was under $2kcal/mol$. Recalling that $\Delta G_{fold} \approx -10$ kcal/mol [30], we deduce that most mutations do not significantly destabilize RBD.

This could be indicative of the universally efficient folding of RBDs seen in nature. The selection pressure acting on the RBD primarily focuses on binding to ACE2 and immune evasion, and therefore the mutations are predominantly on the protein surface and do not significantly affect the protein's stability.

4.4. Analysis of mutations in circulating human SARS-CoV-2 RBDs

All 15,371,428 spike sequences on GISAID [10] as of 14-April-2023 were downloaded and aligned, following approach in the work of Starr et al. [31]. Sequences from non-human origins and with lengths outside $[1260, 1276]$ were removed. They were then aligned via mafft [32] and sequences containing unicode errors, gap or ambiguous characters were removed. Overall, we retained 11,976,984 sequences. RBD amino-acid mutations were enumerated compared to the reference Wuhan-Hu-1 SARS- CoV-2 RBD sequence (Genbank MN908947, residues N331-T531).

We then filtered to remove all sequences with RBD not matching any of the possible intermediates between Wuhan Hu-1 and Omicron BA.1, and obtained 1121 unique oberved RBDs (representing 21% of the initial dataset). Precisely, we allow all possible combination of 15 mutations (G339D, S371L, S373P, S375F, K417N, N440K, G446S, S477N, T478K, E484A,

Q493R, G496S, Q498R, N501Y, Y505H) between Wuhan and Omicron BA.1, which lead to $2^{15} = 32,768$ possible combinations. We measured the count of each RBD as well as the time of its first occurrence, which we approximated by taking 5 % quantile of time data for each RBD.

4.5. Logistic Regression

For the purpose of logistic regression analysis, we utilized the intersecting data obtained from "Methods" RBD Fitness and RBD Binding Affinity. This accumulated dataset comprises 1118 unique RBDs observed in the GISAID database [33], for which the K_D values have been experimentally determined. We further partitioned this data based on the presence or absence of the S:T478K mutation within the sequence, resulting in two distinct subsets.

Ratio between system temperature T_s (corresponding to state of RBD in host) and experimental temperature T_e (corresponding to temperature of experiments conducted in work from Moulana et al. [8, 9], leading to $\Delta G = RT_e ln(K_D)$) was treated as a hyperparameter T (simply refered as "temperature"), that's to say as a parameter whose value is chosen before the fit is done. T was fixed to 1.6, so that fitted concentrations (generally on the order $\sim$ 1 nM to $\sim 10^3$ nM) on the training set generally agree with values of antibody concentrations observed in nature (between 1 and $\sim$ 60 nM in severe symptoms) [34]. We calculated unknown parameters a, C and C_i by fitting:

$$F = a\frac{Ce^{-\ln(K_{DA})/T} + 1}{Ce^{-\ln(K_{DA})/T} + \sum_i C_i e^{-\ln(K_{Dai})/T} + 1} \tag{4}$$

where T is fixed to 1.6 . We emphasize that the choice of this hyperparameter can be done with knowledge of training set alone (and thus does not invalidate prediction capabilities of the model) and that the model behavior is only slightly affected by changes in this hyperparameter (see Supplementary Information: Temperature as a hyperparameter).

Model fitting was performed with least square regression (*scipy.optimize* package) on a randomly selected subset comprising 80% of the existing variants and then evaluated on the remaining 20% for testing absence of overfitting.

To obtain the logistic regression coefficients in Figure 2d, we fitted our model on the whole dataset of existing variants (for which we have the fitness coming from population data). We computed error bars as the standard deviation of coefficients of the model fitted on 10 non-overlapping subsets of existing variants.

4.6. Contributions to fitness and linear regression

To convert improvement of binding to ACE2/immune escape (i.e. change in binding constants) of variants compared to wildtype into a fitness change, we fit a linear regression $\hat{F} = \alpha_0 + \sum_{i\in\{A,ai\}} \alpha_i log(K_{Di})$ to our data ($R^2 = 0.95$). Formally, this boils down to a Taylor expansion of the logistic model, made on the wildtype wt:

$$F_{mut} = F_{wt} + \sum_{j\in\{A,ai\}} \frac{\partial F_{wt}}{\partial log(K_{Dj})} \Delta log(K_{Dj}) \tag{5}$$

where F_{mut} is the fitness of the mutant, $\Delta log(K_{Dj})$ the difference of the logarithm of dissociation constants between mutant and wildtype, and F_{wt} the fitness of the wildtype. Figure 2c shows that most of the experimental data points fall on a near-linear region of the genotype-phenotype map such that a Taylor expansion would provide a reasonable approximation.

To show how scaling of biophysical constant leads to a better selection coefficient for variants, we first computed the difference in biophysical constant, for each variant, compared to wildtype (eg.$\Delta \log(K_{Da}) = \log(K_{Da,mut}) - \log(K_{Da,wild})$), and then multiplied this quantity by the corresponding coefficient α in linear regression. The result for each variant is interpreted as a

fitness increase (eg. $\Delta f_{\log(K_{Da})} = \alpha_{\log(K_{Da})}.\Delta \log(K_{Da})$). For each biophysical constant, we then estimate the contribution of each mutation to the relative fitness increase by regressing it against substitutions features. Formally, we fit for each biophysical constant c: $\Delta f_c = \sum_{m \leq 15} \epsilon_{m,c} X_m$ with $X_m \in \{O, 1\}$ where $\epsilon_{m,c}$ can be interpreted as the contribution of biophysical constant c to the fitness increase given by mutation m (results in Figure 3c). The fitness difference between variant and wildtype is $\Delta F = \sum_c \Delta f_c = \sum_c \sum_m \epsilon_{m,c} X_m = \sum_m (\sum_c \epsilon_{m,c}) X_m$. Thus, $\sum_c \epsilon_{m,c}$ represents the contribution of mutation m to fitness and $\epsilon_{m,c}$ the projection of this contribution on each feature.

4.7. Epistasis analysis

Epistasis describes how mutation interactions can affect the fitness F. If there is no epistasis then the fitness can be described as a linear combinations of the presence of each mutation $X_m \in \{O, 1\}$, leading to a first order epistatic model:

$$F = \sum_i c_i X_i \tag{6}$$

If we consider pairwise epistatic interactions between mutated sites, we get second-order epistatic model:

$$F = \sum_i c_i X_i + \sum_{i<j} c_{ij} X_i X_j \tag{7}$$

c_i are considered as "first-order" epistatic coefficient while $c_{i,j}$ are called "second-order" epistatic coefficients as they are due to epistatic interaction between mutated sites i and j.

To make sure the linear model does not overfit and can generalize on unseen data, we implemented a 10-fold cross-validation strategy (dataset split: 90% / 10%) and identified a linear model involving first and second order coefficients as described in Equation 7 gives a better representation of data than a first order model ($R^2 = 0.98$ vs $R^2 = 0.96$ on test set).

To analyze relationship between second order epistatic coefficients $c_{i,j}$ and distance between mutated sites, we calculated the latter as the Euclidean distance between the average position (computed as the mean of positions of all non-Hydrogen atoms in the amino acid) of each mutated site.

References

1. X. Deng, M. A. Garcia-Knight, M. M. Khalid, V. Servellita, C. Wang, M. K. Morris, A. Sotomayor-González, D. R. Glasner, K. R. Reyes, A. S. Gliwa, N. P. Reddy, C. Sanchez San Martin, S. Federman, J. Cheng, J. Balcerek, J. Taylor, J. A. Streithorst, S. Miller, B. Sreekumar, P.-Y. Chen, U. Schulze-Gahmen, T. Y. Taha, J. M. Hayashi, C. R. Simoneau, G. R. Kumar, S. McMahon, P. V. Lidsky, Y. Xiao, P. Hemarajata, N. M. Green, A. Espinosa, C. Kath, M. Haw, J. Bell, J. K. Hacker, C. Hanson, D. A. Wadford, C. Anaya, D. Ferguson, P. A. Frankino, H. Shivram, L. F. Lareau, S. K. Wyman, M. Ott, R. Andino, and C. Y. Chiu, "Transmission, infectivity, and neutralization of a spike L452R SARS-CoV-2 variant," Cell **184**, 3426–3437.e8 (2021).
2. K. Leung, M. H. Shum, G. M. Leung, T. T. Lam, and J. T. Wu, "Early transmissibility assessment of the N501Y mutant strains of SARS-CoV-2 in the United Kingdom, October to November 2020," Eurosurveillance **26** (2021).
3. S. Cele, I. Gazy, L. Jackson, S.-H. Hwa, H. Tegally, G. Lustig, J. Giandhari, S. Pillay, E. Wilkinson, Y. Naidoo, F. Karim, Y. Ganga, K. Khan, M. Bernstein, A. B. Balazs, B. I. Gosnell, W. Hanekom, M.-Y. S. Moosa, NGS-SA, COMMIT-KZN Team, R. J. Lessells, T. d. Oliveira, and A. Sigal, "Escape of SARS-CoV-2 501Y.V2 from neutralization by convalescent plasma," preprint, Infectious Diseases (except HIV/AIDS) (2021).
4. V. Upadhyay, A. Lucas, S. Panja, R. Miyauchi, and K. M. Mallela, "Receptor binding, immune escape, and protein stability direct the natural selection of SARS-CoV-2 variants," J. Biol. Chem. **297**, 101208 (2021).
5. M. Letko, A. Marzi, and V. Munster, "Functional assessment of cell entry and receptor usage for SARS-CoV-2 and other lineage B betacoronaviruses," Nat. Microbiol. **5**, 562–569 (2020).
6. B. Ju, Q. Zhang, J. Ge, R. Wang, J. Sun, X. Ge, J. Yu, S. Shan, B. Zhou, S. Song, X. Tang, J. Yu, J. Lan, J. Yuan, H. Wang, J. Zhao, S. Zhang, Y. Wang, X. Shi, L. Liu, J. Zhao, X. Wang, Z. Zhang, and L. Zhang, "Human neutralizing antibodies elicited by SARS-CoV-2 infection," Nature **584**, 115–119 (2020).
7. T. N. Starr, A. J. Greaney, S. K. Hilton, D. Ellis, K. H. Crawford, A. S. Dingens, M. J. Navarro, J. E. Bowen, M. A. Tortorici, A. C. Walls, N. P. King, D. Veesler, and J. D. Bloom, "Deep Mutational Scanning of SARS-CoV-2 Receptor Binding Domain Reveals Constraints on Folding and ACE2 Binding," Cell **182**, 1295–1310.e20 (2020).
8. A. Moulana, T. Dupic, A. M. Phillips, J. Chang, S. Nieves, A. A. Roffler, A. J. Greaney, T. N. Starr, J. D. Bloom, and M. M. Desai, "Compensatory epistasis maintains ACE2 affinity in SARS-CoV-2 omicron BA.1," Nat. Commun. **13**, 7011 (2022).
9. A. Moulana, T. Dupic, A. M. Phillips, J. Chang, A. A. Roffler, A. J. Greaney, T. N. Starr, J. D. Bloom, and M. M. Desai, "The landscape of antibody binding affinity in SARS-CoV-2 omicron BA.1 evolution," Elife **12** (2023).
10. S. Elbe and G. Buckland-Merrett, "Data, disease and diplomacy: GISAID's innovative contribution to global health: Data, Disease and Diplomacy," Glob. Challenges **1**, 33–46 (2017).
11. N. Chéron, A. W. R. Serohijos, J.-M. Choi, and E. I. Shakhnovich, "Evolutionary dynamics of viral escape under antibodies stress: A biophysical model," Protein Sci. **25**, 1332–1340 (2016).
12. A. Rotem, A. W. R. Serohijos, C. B. Chang, J. T. Wolfe, A. E. Fischer, T. S. Mehoke, H. Zhang, Y. Tao, W. Lloyd Ung, J.-M. Choi, J. V. Rodrigues, A. O. Kolawole, S. A. Koehler, S. Wu, P. M. Thielen, N. Cui, P. A. Demirev, N. S. Giacobbi, T. R. Julian, K. Schwab, J. S. Lin, T. J. Smith, J. M. Pipas, C. E. Wobus, A. B. Feldman, D. A. Weitz, and E. I. Shakhnovich, "Evolution on the biophysical fitness landscape of an RNA virus," Mol. Biol. Evol. **35**, 2390–2400 (2018).
13. F. Pucci and M. Rooman, "Prediction and Evolution of the Molecular Fitness of SARS-CoV-2 Variants: Introducing SpikePro," Viruses **13**, 935 (2021).
14. F. Obermeyer, M. Jankowiak, N. Barkas, S. F. Schaffner, J. D. Pyle, L. Yurkovetskiy, M. Bosso, D. J. Park, M. Babadi, B. L. MacInnis, J. Luban, P. C. Sabeti, and J. E. Lemieux, "Analysis of 6.4 million SARS-CoV-2 genomes identifies mutations associated with fitness," Science **376**, 1327–1332 (2022).
15. C. S. Wylie and E. I. Shakhnovich, "A biophysical protein folding model accounts for most mutational fitness effects in viruses," Proc. Natl. Acad. Sci. U. S. A. **108**, 9916–9921 (2011).
16. J. V. Rodrigues, S. Bershtein, A. Li, E. R. Lozovsky, D. L. Hartl, and E. I. Shakhnovich, "Biophysical principles predict fitness landscapes of drug resistance," Proc. National Acad. Sci. **113** (2016).
17. L. I. Gong, M. A. Suchard, and J. D. Bloom, "Stability-mediated epistasis constrains the evolution of an influenza protein," eLife **2**, e00631 (2013).
18. J. M. Fonville, S. H. Wilks, S. L. James, A. Fox, M. Ventresca, M. Aban, L. Xue, T. C. Jones, null, null, null, Y. Wong, A. Mosterin, L. C. Katzelnick, D. Labonte, null, G. van der Net, E. Skepner, C. A. Russell, T. D. Kaplan, G. F. Rimmelzwaan, N. Masurel, J. C. de Jong, A. Palache, W. E. P. Beyer, null, null, H. F. L. Wertheim, A. C. Hurt, A. D. M. E. Osterhaus, I. G. Barr, R. A. M. Fouchier, P. W. Horby, and D. J. Smith, "Antibody landscapes after influenza virus infection or vaccination," Science **346**, 996–1000 (2014).
19. E. Y. Klein, D. Blumenkrantz, A. Serohijos, E. Shakhnovich, J.-M. Choi, J. V. Rodrigues, B. D. Smith, A. P. Lane, A. Feldman, and A. Pekosz, "Stability of the influenza virus hemagglutinin protein correlates with evolutionary dynamics," mSphere **3** (2018).
20. X. Wei and J. Zhang, "Patterns and Mechanisms of Diminishing Returns from Beneficial Mutations," Mol. Biol. Evol. **36**, 1008–1021 (2019).
21. H.-H. Chou, H.-C. Chiu, N. F. Delaney, D. Segrè, and C. J. Marx, "Diminishing Returns Epistasis Among Beneficial Mutations Decelerates Adaptation," Science **332**, 1190–1192 (2011).
22. S. Kryazhimskiy, D. P. Rice, E. R. Jerison, and M. M. Desai, "Global epistasis makes adaptation predictable despite sequence-level stochasticity," Science **344**, 1519–1522 (2014).

23. A. W. R. Serohijos and E. I. Shakhnovich, "Contribution of selection for protein folding stability in shaping the patterns of polymorphisms in coding regions," Mol. Biol. Evol. **31**, 165–176 (2014).
24. D. M. Lyons, Z. Zou, H. Xu, and J. Zhang, "Idiosyncratic epistasis creates universals in mutational effects and evolutionary trajectories," Nat. Ecol. & Evol. **4**, 1685–1693 (2020).
25. J. V. Rodrigues, S. Bershtein, A. Li, E. R. Lozovsky, D. L. Hartl, and E. I. Shakhnovich, "Biophysical principles predict fitness landscapes of drug resistance," Proc. Natl. Acad. Sci. U. S. A. **113**, E1470–8 (2016).
26. F. Touret, L. Luciani, C. Baronti, M. Cochin, J.-S. Driouich, M. Gilles, L. Thirion, A. Nougairède, and X. de Lamballerie, "Replicative Fitness of a SARS-CoV-2 20I/501Y.V1 Variant from Lineage B.1.1.7 in Human Reconstituted Bronchial Epithelium," mBio **12**, e00850–21 (2021).
27. R. Burioni and E. J. Topol, "Has SARS-CoV-2 reached peak fitness?" Nat. Med. **27**, 1323–1324 (2021).
28. N. Matange, S. Hegde, and S. Bodkhe, "Adaptation Through Lifestyle Switching Sculpts the Fitness Landscape of Evolving Populations: Implications for the Selection of Drug-Resistant Bacteria at Low Drug Pressures," Genetics **211**, 1029–1044 (2019).
29. L. Montanucci, E. Capriotti, Y. Frank, N. Ben-Tal, and P. Fariselli, "DDGun: an untrained method for the prediction of protein stability changes upon single and multiple point variations," BMC Bioinform. **20**, 335 (2019).
30. N. Tokuriki, F. Stricher, J. Schymkowitz, L. Serrano, and D. S. Tawfik, "The Stability Effects of Protein Mutations Appear to be Universally Distributed," J. Mol. Biol. **369**, 1318–1332 (2007).
31. T. N. Starr, A. J. Greaney, A. Addetia, W. W. Hannon, M. C. Choudhary, A. S. Dingens, J. Z. Li, and J. D. Bloom, "Prospective mapping of viral mutations that escape antibodies used to treat COVID-19," Science **371**, 850–854 (2021).
32. K. Katoh and D. M. Standley, "MAFFT Multiple Sequence Alignment Software Version 7: Improvements in Performance and Usability," Mol. Biol. Evol. **30**, 772–780 (2013).
33. S. Elbe and G. Buckland-Merrett, "Data, disease and diplomacy: GISAID's innovative contribution to global health," Glob Chall **1**, 33–46 (2017).
34. K. A. de Jong, H. Rosing, M. Vermunt, A. D. Huitema, and J. H. Beijnen, "Quantification of anti-SARS-CoV-2 antibodies in human serum with LC-QTOF-MS," J. Pharm. Biomed. Anal. **205**, 114319 (2021).

Acknowledgements

We gratefully acknowledge all data contributors, i.e., the Authors and their Originating laboratories responsible for obtaining the specimens, and their Submitting laboratories for generating the genetic sequence and metadata and sharing via the GISAID Initiative, on which this research is based.

We would like to thank Vaibhav Upadhyay, Krishna Malella, Zechen Zhang and Junlang Liu for useful discussions.

Author contributions

D.W., M.H., V.M. and E.I.S conceived and designed the experiments. D.W., M.H. and V.M. performed the experiments. D.W., M.H. and V.M. analyzed the data. E.I.S supervised the work. D.W., M.H. and V.M. wrote the paper.

Competing interests

The authors declare no competing interests.

Table 1. Terminology. A summary of terms and their representations used in the paper. The first column (left) provides the term used and its description, while the second column (right) has the corresponding mathematical symbol and equation where relevant

Term	Representation
Free Energy of RBD	
- Unfolded	G_u
- Folded and unbound	G_f
- Folded and bound to ACE2	G_{bA}
- Folded and bound to antibody i	G_{ai}
Boltzmann factor	$\beta = \frac{1}{k_B T_s}$
Concentration	[...]
Free energy difference	
- Folding	$\Delta G_{\text{fold}} = G_f - G_u$
- ACE2 binding	$\Delta G_A = G_{bA} - G_f$
- Antibody i binding	$\Delta G_{ai} = G_{ai} - G_f$
Dissociation constant for binding to	
- ACE2	K_{DA}
- Antibody i	K_{Dai}
Fitness of the mutant	F_{mut}
Fitness of the wild-type	F_{wild}
Relative fitness	F